Science Advances
AAAS

advances.sciencemag.org/cgi/content/full/3/3/e1601749/DC1

Supplementary Materials for

Air pollution–aerosol interactions produce more bioavailable iron for ocean ecosystems

Weijun Li, Liang Xu, Xiaohuan Liu, Jianchao Zhang, Yangting Lin, Xiaohong Yao, Huiwang Gao, Daizhou Zhang, Jianmin Chen, Wenxing Wang, Roy M. Harrison, Xiaoye Zhang, Longyi Shao, Pingqing Fu, Athanasios Nenes, Zongbo Shi

Published 1 March 2017, *Sci. Adv.* **3**, e1601749 (2017)
DOI: 10.1126/sciadv.1601749

This PDF file includes:

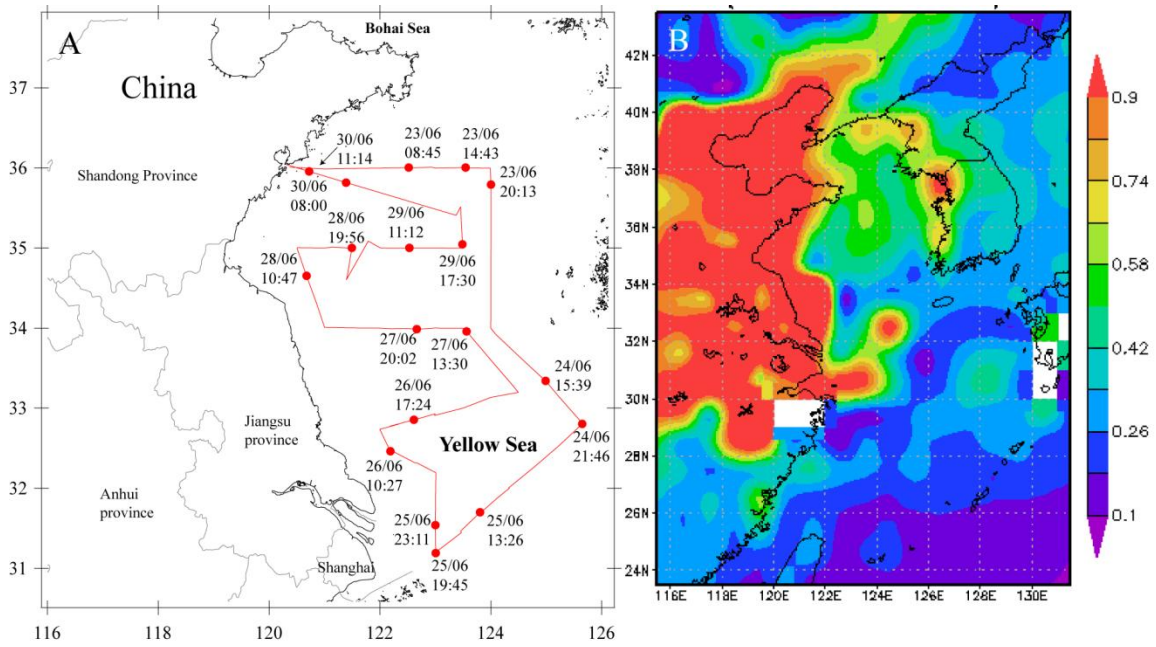

fig. S1. Cruise route and AOD map. (**A**) Cruise route in the Yellow sea and 18 sampling sites during 23 June – 30 June, 2013. The sampling date and time (Beijing time) were annotated for each sampling station (**B**) AOD map derived from MODIS-terra data during 20 - 30 June, 2013. There is a clear gradient of AOD from the mainland China to the Yellow Sea.

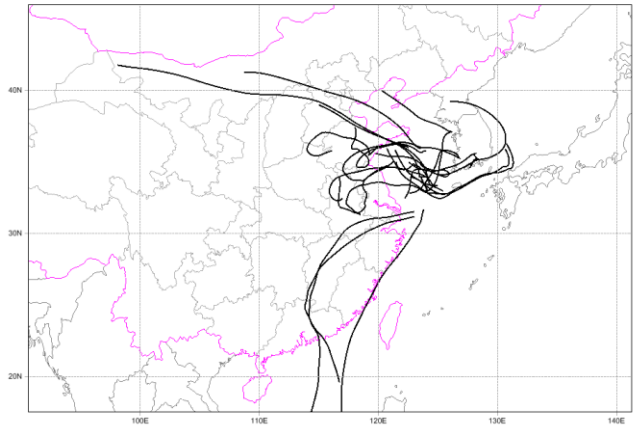

fig. S2. Air mass back trajectories at 1500 m of each sampling station over the Yellow sea. A majority of these air masses reaching the sampling sites were from East China.

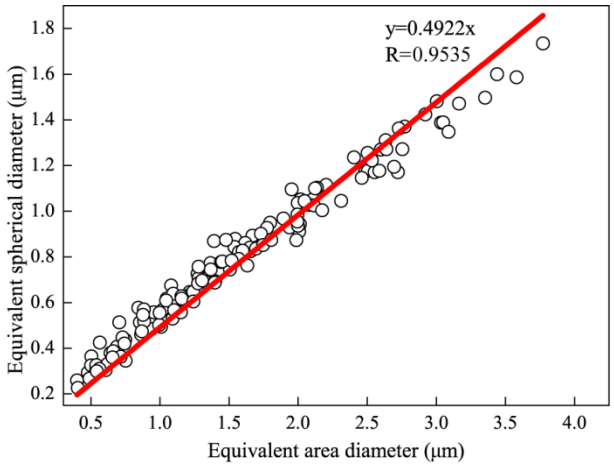

fig. S3. The correlation of ESD and EAD based on AFM analysis. The correlation coefficient was used to calculate the ESD of particles from the EAD obtained from Transmission Electron Microscope.

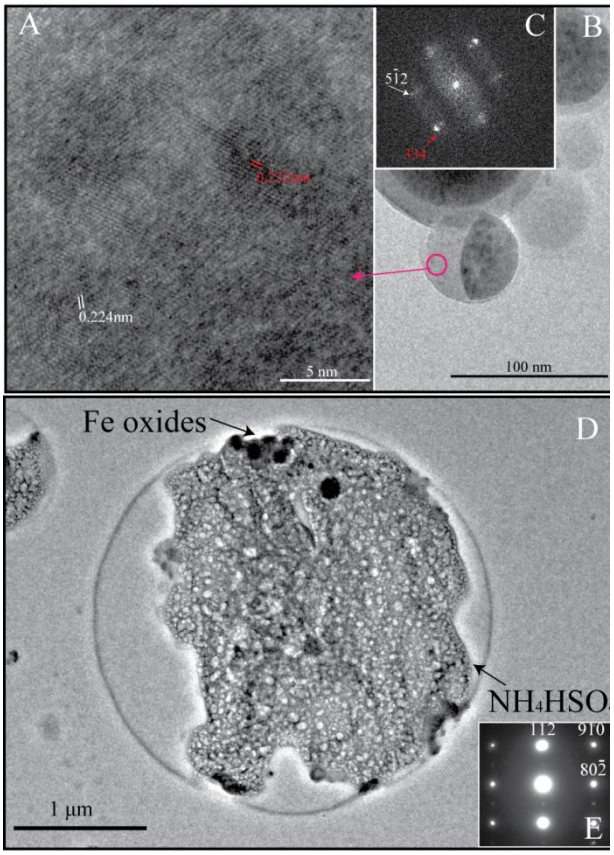

fig. S4. TEM micrographs of an Fe-rich particle and a sulfate particle collected over East China Sea. (**A**) High resolution micrograph of an Fe-rich particle shown in Figure S4B; (**B**) Low resolution TEM micrograph of the Fe-rich particle; (**C**) fast fourier transforms (FFTs) of the Fe-rich particle based on the high-resolution micrograph in Figure S4A, which was compared with a simulated diffraction pattern of Orthorhombic magnetite (space group: Pmc21, no. 26) to determine the dominant lattice spacings of the Fe-rich particle; indexing of the lattice fringes of the Fe-rich particles is consistent with (57-9) crystal zone axis of magnetite; (**D**) TEM micrograph of a sulfur-containing particle; (**E**) SAED pattern of the sulfur-containing particle in (D), consistent with (-19-4) crystal zone axis of ammonium bisulfate; this confirms the presence of ammonium bisulfate (monoclinic, a=24.48, b=4.58, c=14.75).

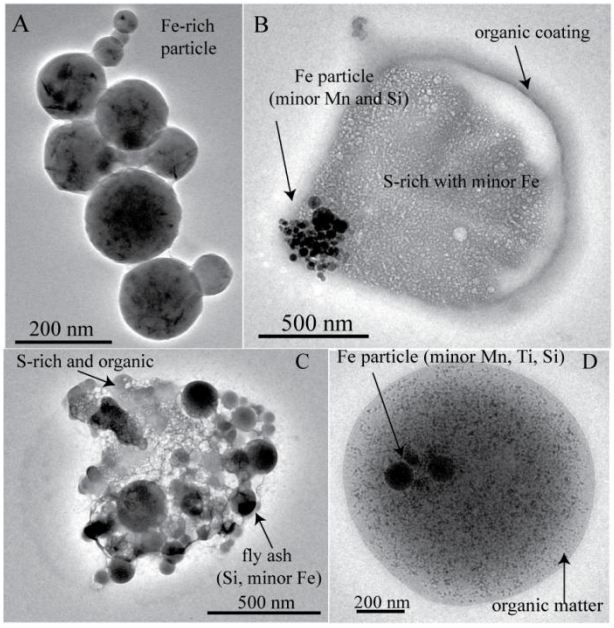

fig. S5. Morphology and mixing state of Fe-rich and fly ash particles. (**A**) An externally mixed Fe-rich particle; (**B**) Fe-rich particle aggregate internally mixed with sulfate and organic matter; (**C**) Fly ash aggregates internally mixed with sulfate and organic matter; (**D**) Fe-rich particle aggregates internally mixed with organic matter (with a small amount of S).

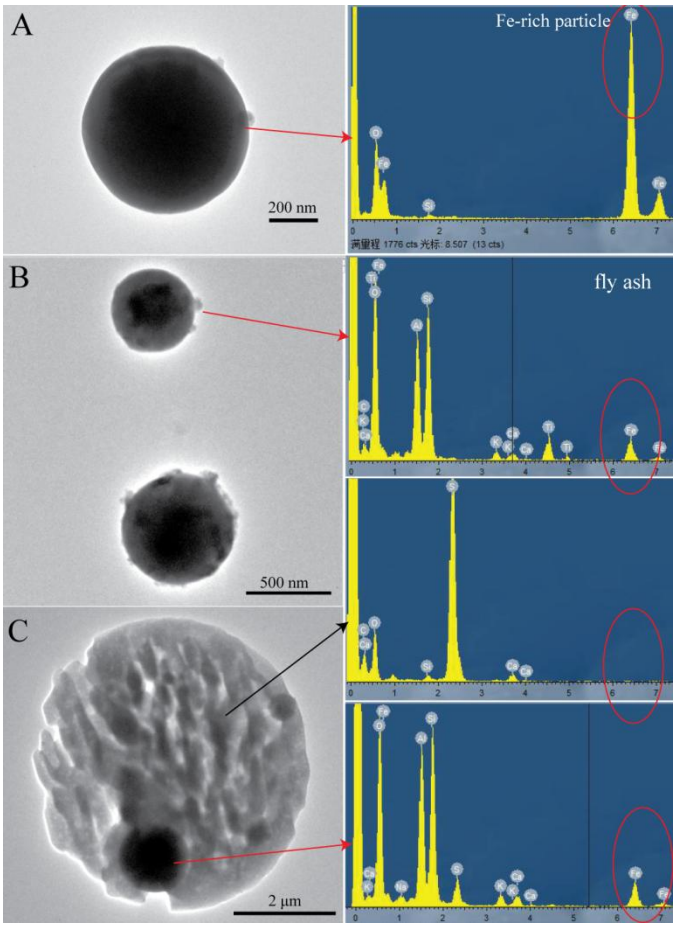

fig. S6. TEM image of Fe-rich and coal fly ash particles collected in sources. (**A**) An Fe-rich particle collected from a steelwork; (**B**) Coal fly ash particles collected from coal-fired plant; Energy Dispersive X-ray Spectrometry (EDS) analysis showed that the fly ash particle is mainly composed of Si and Al with a small amount of Fe; (**C**) An aerosol particle generated from fly ash and ammonium sulfate solution at pH=5.6 (Exp. 3, see Methods). No Fe is detected in the sulfate matrix.

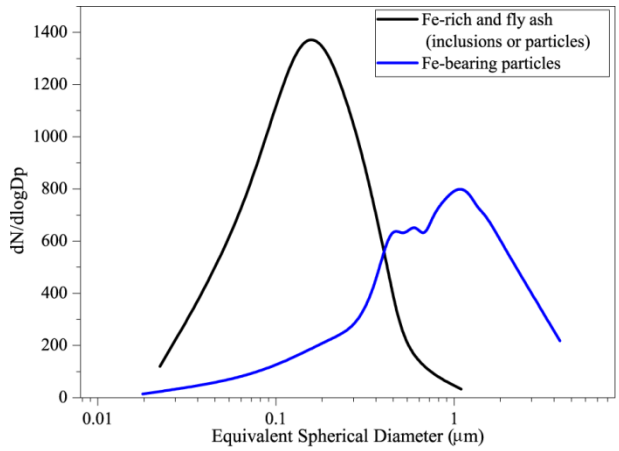

fig. S7. Size distributions of Fe-rich and fly ash inclusions only (excluding secondary coatings) and Fe-bearing particles.

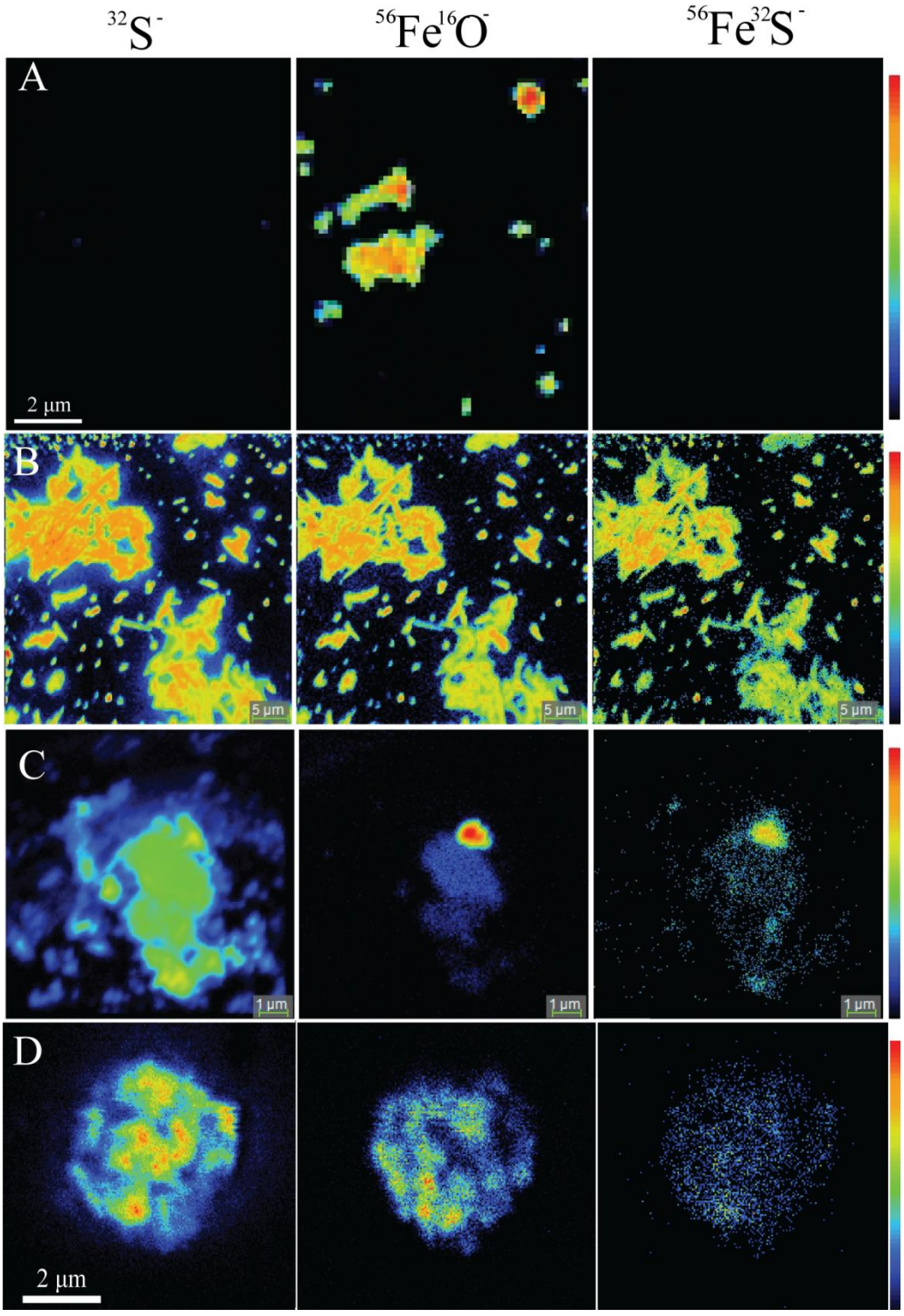

fig. S8. NanoSIMS ion intensity of S^-, FeO^-, and FeS^- in standard samples. (**A**) hematite (Fe_2O_3); (**B**) Fe(III) sulfate; (**C**) a particle generated from hematite and sulfuric acid (pH=2) suspension (Exp. 1); and (**D**) a particle generated from hematite and sulfuric

and oxalic acid (pH = 1.8) suspension (Exp. 2). No S^- and FeS^- signals were detected in hematite (A); the ion intensity ratio of S^-:FeO^-+FeS^- and FeS^-:FeO^-+FeS^- are 7 and 0.2 for pure $Fe_2(SO_4)_3$ powder (B), 366 and 0.1 for the particle generated from hematite and sulfuric acid suspension (D), and 83 and 0.3 in the particle generated from hematite and sulfuric and oxalic acid suspension (D).

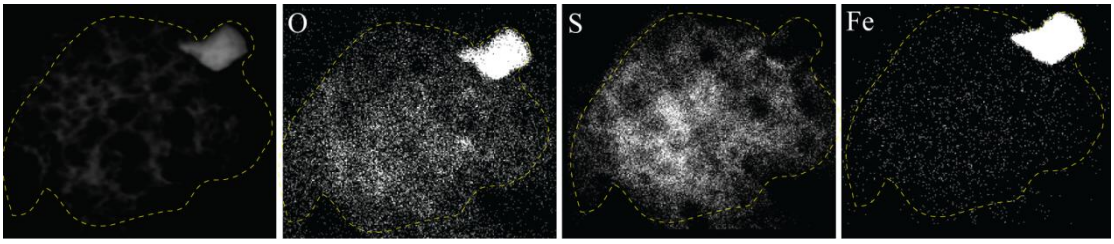

fig. S9. Dark-field image and elemental mapping of an individual hematite-bearing particle (Exp. 1). The hotspot is a hematite particle. Fe is detected in the sulfate coating, which can only came from Fe solubilized from the hematite particle.

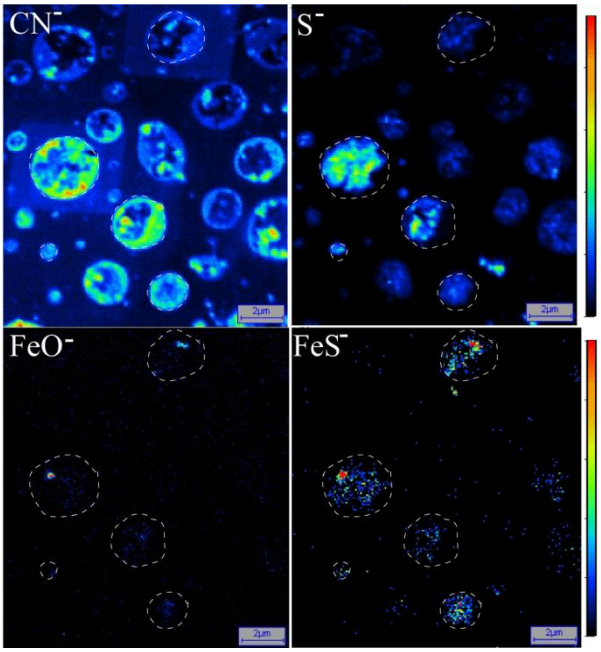

fig. S10. NanoSIMS ion intensity of C^-, CN^-, S^-, FeO^-, and FeS^- in individual particles collected over Yellow Sea. FeS^- signal was clearly detected in the sulfate coating around the FeO^- hotspots, likely Fe-rich or fly ash particles.

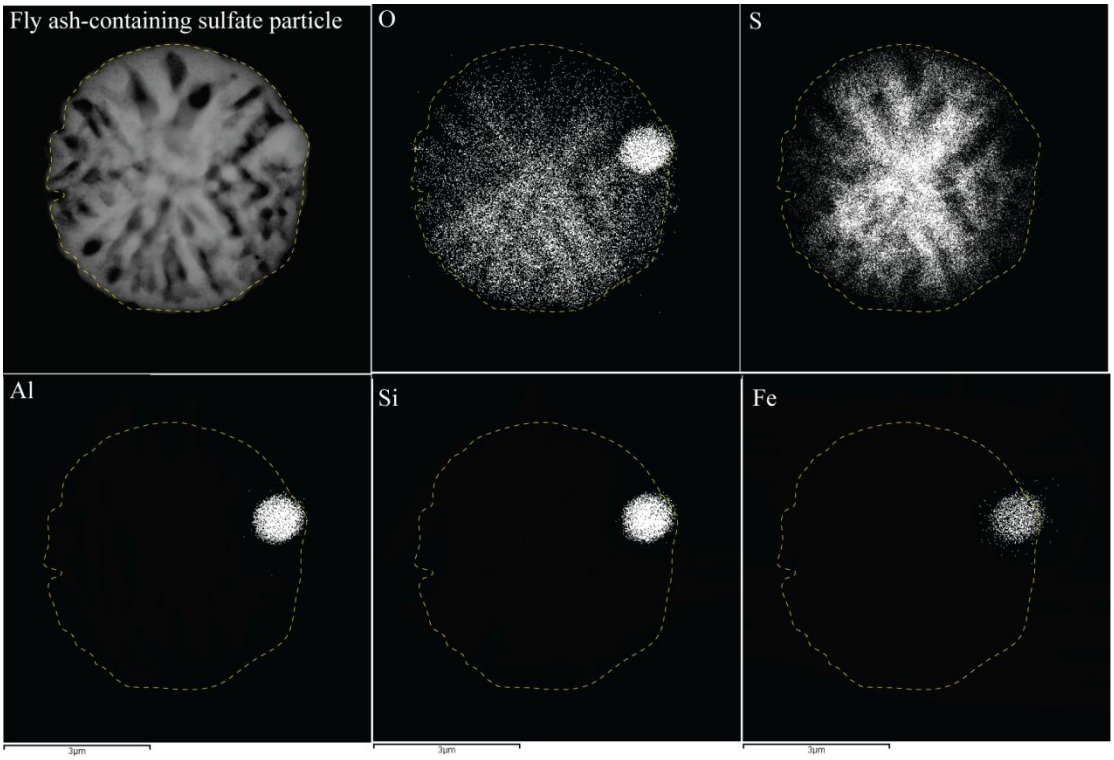

fig. S11. Dark-field image and elemental mapping of an internally mixed particle generated from ammonium sulfate solution (pH 5.6) mixed with coal fly ash. The hotspot in O, Al, Si and Fe maps was indicative of a coal fly ash particle. No Fe was detected in the sulfate coating (Fe mapping), indicating that there is no detectable soluble Fe in the coal fly ash.